

## Effects of Deformation Rate on the Unbinding Pathway of the MMP8-Aggrecan\_IGD Complex in Cartilage

Deng Li<sup>1</sup> and Shuwei Chang<sup>1,\*</sup>

**Abstract:** Mechanical force plays a critical role in the remodeling and degradation of cartilage tissues. The cartilage tissue generates, absorbs, and transmits mechanical force, enabling specific biological processes in our body. A moderate intensity mechanical force is necessary for cartilage tissue remodeling and the adaptation of biomechanical properties, but a high intensity mechanical force can lead to pathological degradation of cartilage tissue. However, the molecular mechanism of cartilage degradation is still unclear. We use full atomistic simulations with SMD simulations to investigate whether the magnitude of mechanical force affects the unbinding pathway of the MMP8-Aggrecan\_IGD complex. We find that when the pulling velocity is slow, the mechanical force required to unbind the Aggrecan\_IGD from MMP8 is higher, and a three-step unbinding pathway is observed. On the other hand, when the pulling velocity is fast, the mechanical force required to unbind the Aggrecan\_IGD from MMP8 is lower, and a two-step unbinding pathway is observed. Our results help us to understand how the magnitude of the mechanical force affects the unbinding pathway of the enzyme-ligand complex in cartilage tissue at the molecular level.

**Keywords:** Mechanical force, steered molecular dynamics (SMD), unbinding pathway, potential of mean force (PMF).

### 1 Introduction

Cartilage tissue is an important structural component in our body, providing biomechanical properties for joints [Fosang, Rogerson, East et al. (2008); Pratta, Yao, Decicco et al. (2003)]. Mechanical force plays a critical role in the remodeling and degradation of cartilage tissues [Grodzinsky, Levenston, Jin et al. (2000)]. The cartilage tissue generates, absorbs and transmits mechanical force, enabling specific biological process in our body [Julkunen, Harjula, Iivarinen et al. (2009); Borrelli, Torzilli, Grigiene et al. (1997)]. These biological processes are strongly influenced by biomechanical signals mediated by mechanical forces [Pufe, Lemke, Kurz et al. (2004)]. A moderate intensity mechanical force is necessary for cartilage tissue remodeling and the adaptation of biomechanical properties, but a high intensity mechanical force can lead to pathological degradation of cartilage tissue and cause related diseases such as developmental dysplasia of the hip (DDH) and osteoarthritis (OA) [Ewers, Jayaraman, Banglmaier et al. (2003); O’Kane, Hutchinson,

---

<sup>1</sup> Department of Civil Engineering, National Taiwan University, Taipei 10617, Taiwan.

\* Corresponding Author: Shuwei Chang. Email: changsw@ntu.edu.tw.

Atley et al. (2006); Basse, Rothwell, Littlewood et al. (1998); Ewers, Dvoracek-Driksna, Orth et al. (2001); Muller and Seddon (1953)].

Aggrecan is one of the dominant extracellular matrix (ECM) constituents in cartilage tissues providing relatively low friction for smooth articular movement [Venn and Maroudas (1977)]. Aggrecan degradation in cartilage tissue occurs predominantly through proteolysis and has been attributed to the action of ADAMTS (a disintegrin and metalloproteinase with thrombospondin motifs) and MMPs (matrix metalloproteinases) [Durigova, Nagase, Mort et al. (2011); Malemud (2017)]. Many diseases are associated with pathological degradation of aggrecan caused by high intensity mechanical force [Buckwalter (2012); Felson (2013); Huang and Wu (2008)]. During the degradation of aggrecan, the enzymes bind to specific sites in the interglobular domain (IGD) of the aggrecan core protein and form a protein-ligand complex for further hydrolyzing [Huang and Wu (2008); Durigova, Nagase, Mort et al. (2011)]. However, it remains unclear on how the mechanical forces may affect the molecular structures of the enzyme and the ECM in cartilage.

Full atomistic simulations with steered molecular dynamics (SMD) simulations have been successfully used to investigate the unbinding pathway of many protein-ligand complexes (Tab. 1) [Dellago and Hummer (2013); Ferreira, Franca and Leite (2017); Patel, Berteotti, Ronsisvalle et al. (2014); Shen, Guan, Xu et al. (2012); Tekpinar (2018); Vashisth and Abrams (2008); Zhang, Santos, Zhou et al. (2016)]. In the SMD simulations, an external force or a constant velocity is applied to the system, and the responses of the system are recorded and analyzed. SMD simulations allow us to apply mechanical forces on the ligands to investigate the unbinding pathway and the conformation changes of the protein-ligand complex from its equilibrium state to accelerate the transitions between different local energy minima [Aprodu, Redaelli and Soncini (2008)].

The objective of this study is to understand the effects of mechanical force on the unbinding pathway of the MMP8-Aggrecan\_IGD complex. We combine the peptide of a representative cleavage site in the aggrecan IGD with MMP8 to form MMP8-Aggrecan\_IGD complex [Humphrey, Dalke and Schulten (1996)]. Full atomistic simulations with SMD simulations are performed to investigate whether the magnitude of mechanical force affects the unbinding pathway of the MMP8-Aggrecan\_IGD complex. Simulations with different SMD parameters, including different force constants and pulling velocities, are performed to explore the effects of different mechanical force and potential of mean force (PMF) is calculated to identify the difference of energy profile.

## **2 Computational details**

The real sequences of aggrecan core protein in the interglobular domain of human are used to generate the aggrecan core protein peptide. The sequences of the aggrecan core protein in the interglobular domain (Aggrecan\_IGD) are obtained from the UniProt protein database (<http://www.uniprot.org/uniprot/P16112>) [Renaux and Consortium (2018)]. The chosen sequences are PDMELPLPRNITEGE~ARGSVILTVKPIFEV. The scissile bond is depicted with a~sign. The homology model of Aggrecan\_IGD is constructed using Modeller 9.19 [Fiser and Sali (2003)]. NAMD 2.12 with CHARMM27 force field is used for all the simulations [Phillips, Braun, Wang et al. (2005); MacKerell, Bashford, Bellott et al. (1998); Jo, Cheng, Islam et al. (2014)]. The homology model is energy minimized with conjugate

gradient scheme, and the initial structure of the MMP8 catalytic domain is adapted from the protein data bank of PDB ID: 2OY4 [Bertini, Calderone, Fragai et al. (2006)]. The MMP8 and Aggrecan\_IGD are combined to form MMP8-Aggrecan\_IGD complex by using Visual Molecular Dynamics program [Humphrey, Dalke and Schulten (1996)]. The MMP8-Aggrecan\_IGD complex is solvated by using the TIP3P water molecules. Ions are added to the model to neutralize the simulation system (Fig. 1). After the model construction, the complex is first energy minimized with conjugate gradient algorithm, followed by NPT equilibration for 80 ns at a constant temperature of 310 K and with 1 bar pressure. Simulation trajectories from 50 ns to 70 ns are used to analyze.

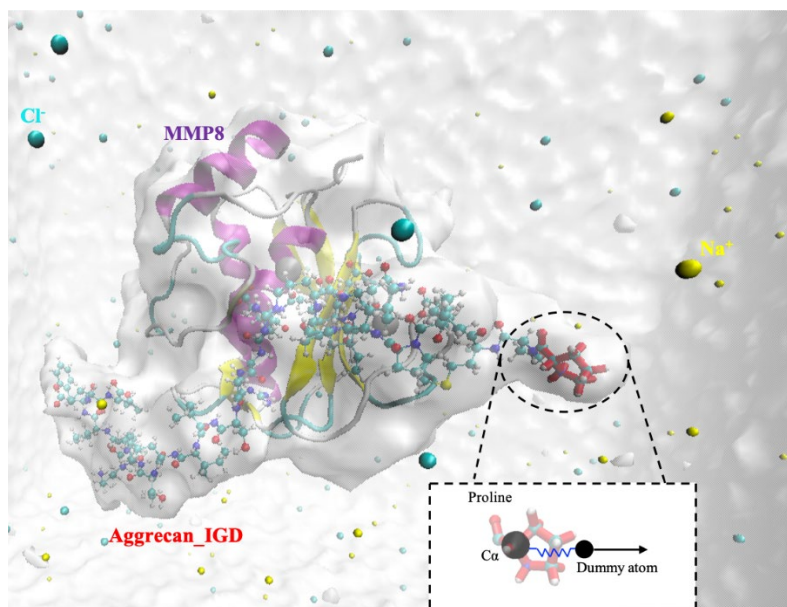


**Figure 1:** MMP8-Aggrecan\_IGD complex solvated in water box which rendered in molecular surface renderer called MSMS [Sanner, Olson and Spehner (1996)]. The complex used for the SMD simulation consists of MMP8 which rendered in NewCartoon and Aggrecan\_IGD ligand which rendered in CPK. Chloride and sodium ions are shown in light blue and yellow. The constant velocity is applied at the C $\alpha$  atom of the first residue of the Aggrecan\_IGD ligand

To study the effects of different mechanical forces, we perform SMD simulations with different pulling velocities. In the constant velocity SMD, pulling velocity has a significant influence on the magnitude of the unbinding force. In the previous studies, there have been various velocities adapted in different SMD studies (Tab. 1). In order to mimic the atomic force microscopy experiment, the pulling velocity used in the SMD simulation should be as slow as possible. On the other hand, the force constant should be large enough to be able to measure the local dissociation potential; however, it should not be too large as the fluctuation of the force-displacement curve increases as the force constant increases. The choice of pulling velocities and force constant are based on a balance between computer resource and accuracy. We chose two different pulling velocities: 0.01 Å/ps and 0.05 Å/ps,

both with a force constant of  $7 \text{ kcal/mol/\AA}^2$ , to investigate the effects of the magnitude of the mechanical forces. The MMP8 is fixed during the SMD simulations. To obtain reliable PMF profiles of the Aggrecan\_IGD dissociation from MMP8, a number of additional simulations are conducted by repeating the SMD trajectories. Ten SMD trajectories are generated for each PMF calculation. Based on the protocol of Christoph Dellago et al. [Dellago and Hummer (2013)], we use second order cumulant expansion of Jarzynski's equality to calculate the PMF [Jarzynski (1997); Crooks (2000); West, Olmsted and Paci (2006); Dellago and Hummer (2013)].

**Table 1:** The choice of force constant and velocity in different SMD study

Protein	Ligand	Force constant, K	Velocity, v ( $\text{\AA}/\text{ps}$ )	Reference
5-enolpyruvylshikimate 3-phosphate synthase (EPSPs)	Glyphosate	$367 \text{ kJ/mol/nm}^2$	0.01	[Ferreira, Franca and Leite (2017)]
Carbonic anhydrase (CA)	Coumarin2 5Z/5E	500, 1000 pN/ $\text{\AA}$	0.02	[Tekpinar (2018)]
Human pulmonary surfactant protein D (SP-D)	$\alpha$ -D-glucose	$0.5 \text{ kcal/mol/\AA}^2$	0.05	[Zhang, Zheng and Zhang (2010)]
$\beta$ -hydroxyacyl-ACP dehydratase of Pf (P/FabZ)	Monohydroxylated flavones and polyhydroxylated flavones	$7 \text{ kcal/mol/\AA}^2$	0.0005	[Colizzi, Perozzo, Scapozza et al. (2010)]
Hsc70 (Hsp70)	Auxilin (Hsp40)	$300 \text{ kJ/mol/nm}^2$	0.02	[Xue, Zhou, Sun et al. (2017)]
human vascular endothelial growth factor receptor 2 (VEGFR2)	Sorafenib and sunitinib	$15 \sim 35 \text{ kcal/mol/\AA}^2$	$0.0001 \sim 0.01$	[Capelli and Costantino (2014)]
$\beta$ -lactamase protein	Totally 23 small compounds	$600 \text{ kJ/mol/nm}^2$	0.05	[Truong and Li (2018)]
ssDNA and dsDNA with acetone, ethanol	Adenine (A), Guanine (G), Cytosine (C), and Thymine (T)	$10 \text{ kcal/mol/\AA}^2$	0.1	[Zhang, Wang and Cranford (2016)]
Insulin	Phenol	$5 \text{ kcal/mol/\AA}^2$	0.01	[Vashisth and Abrams (2008)]
DnaK <sup>WT</sup> and DnaK <sup>L484W</sup>	Peptide NRLLLTG	$300 \text{ kJ/mol/nm}^2$	0.01	[Xu, Hasin, Shen et al. (2013)]
Cyclin-dependent kinase 5 (CDK5)	Totally nine inhibitors	$100 \text{ kcal/mol/\AA}^2$	0.007	[Patel, Berteotti, Ronsisvalle et al. (2014)]

**Table 1:** Continued

B-RAF kinase	PLX4720 and TAK-632	20 ~ 50 kcal/mol/Å <sup>2</sup>	0.0006	[Niu, Li, Pan et al. (2016)]
MDM2-p53	Totally four ligands	0.2 kcal/mol/Å <sup>2</sup>	0.01	[Hu, Xu and Wang (2015)]
CYP2E1	Indazole	4 kcal/mol/Å <sup>2</sup>	0.01	[Shen, Cheng, Xu et al. (2012)]
Estrogen receptors (ERs)	Way-244 and (b) Genistein	10 kcal/mol/Å <sup>2</sup>	0.02	[Shen, Li, Liu et al. (2009)]
Matrix metalloproteinase-9 (MMP-9)	Hinokiflavone and Arctiin.	500 kJ/mol/nm <sup>2</sup>	0.00005	[Kalva, Azhagiya Singam, Rajapandian et al. (2014)]

### 3 Result and discussion

#### 3.1 Molecular structure of the MMP8-Aggrecan\_IGD complex

To analyze the structural stability of the MMP8-Aggrecan\_IGD complex, the root-mean-square deviations (RMSD) are calculated. The RMSD from the initial equilibrium state of the MMP8, Aggrecan\_IGD, and MMP8-Aggrecan\_IGD complex are shown as a function of simulation time in Fig. 2. The RMSD profiles show that the structural conformation of the complex reaches a stable conformation at 25 ns. The average RMSD of the MMP8-Aggrecan\_IGD complex is 2.61 Å, with a standard deviation of 0.26 Å. The average RMSD of the MMP8 is 2.44 Å, with a standard deviation of 0.25 Å. The differences of RMSD between the MMP8-Aggrecan\_IGD complex and the MMP8 is only 0.17 Å suggesting that the binding of Aggrecan\_IGD does not alter the molecular structure of MMP8 significantly.

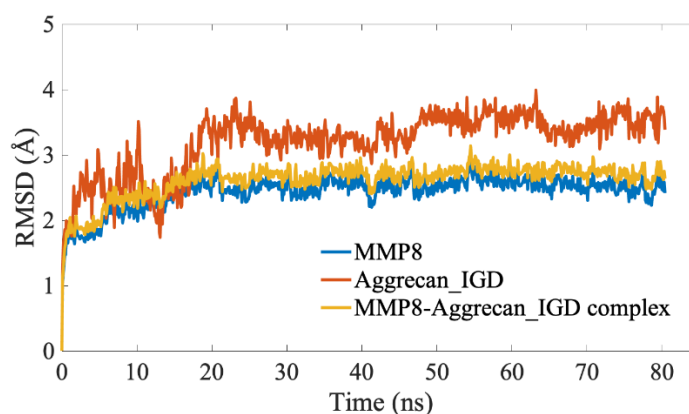


**Figure 2:** Root-mean-square deviations (RMSD) with respect to the initial equilibrium state for MMP8-Aggrecan\_IGD complex

We analyze the hydrogen bonds of MMP8-Aggreca\_n\_IGD complex with a distance cut-off of 3.5 Å and an angle cut-off of 30°. Aggreca\_n\_IGD bound MMP8 mainly through five hydrogen bonds: Tyr<sub>219</sub>-O··HN-Ile<sub>21</sub>, Glu<sub>180</sub>-O··HN-Arg<sub>17</sub>, Gly<sub>158</sub>-O··HN-Arg<sub>17</sub>, Leu<sub>160</sub>-NH··O-Glu<sub>15</sub> and Ala<sub>161</sub>-O··HN-Glu<sub>15</sub>. The number of hydrogen bonds between the MMP8 and the Aggreca\_n\_IGD is plotted as a function of simulation time in Fig. 3. It is shown that the number of hydrogen bonds has a large fluctuation in the first 25 ns simulations. After 25 ns, the number of hydrogen bonds approaches a stable value of 4.7815. The results of the RMSD and the number of hydrogen bonds confirms that our simulation reaches a stable structure for SMD simulations.

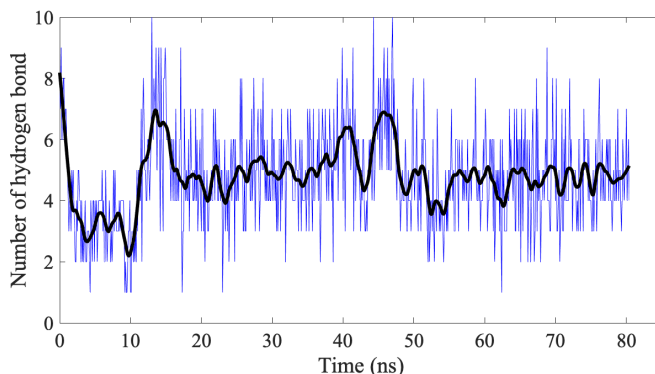


**Figure 3:** The number of hydrogen bonds (blue line) between the MMP8 and the Aggreca\_n\_IGD as a function of the simulation time

### 3.2 Effects of pulling velocity on the unbinding pathway

SMD simulations are performed to investigate the unbinding pathway to provide molecular insights into the interactions between the MMP8 and the Aggreca\_n\_IGD. Force-reaction coordinate curves and the number of hydrogen bonds are analyzed to investigate the unbinding pathway of MMP8-Aggreca\_n\_IGD complex at different pulling velocity [Dellago and Hummer (2013); Ferreira, Franca and Leite (2017); Patel, Berteotti, Ronsisvalle et al. (2014); Shen, Guan, Xu et al. (2012); Tekpinar (2018); Vashisth and Abrams (2008); Zhang, Santos, Zhou et al. (2016)].

The force-reaction coordinate curve of the MMP8-Aggreca\_n\_IGD complex at a pulling velocity of 0.01 Å/ps is shown in Fig. 4. There are three peaks on the force-reaction coordinate curve during the SMD simulation. The first peak occurs at a reaction coordinate of 24 Å. The second peak is at the reaction coordinate of 35 Å. The maximum peak appears at 46 Å. At about 55 Å, the Aggreca\_n\_IGD is completely pulled out from the MMP8, and thus the pulling forces go to zero.

Fig. 5 shows the unbinding pathway of the MMP8-Aggreca\_n\_IGD complex at the pulling velocity of 0.01 Å/ps. Fig. 5(A) shows the structure of MMP8-Aggreca\_n\_IGD complex before applying mechanical force. When pulling Aggreca\_n\_IGD out of the MMP8 catalytic domain, the Aggreca\_n\_IGD first lost two hydrogen bonds: Ala<sub>161</sub>-O··HN-Glu<sub>15</sub> and Leu<sub>160</sub>-NH··O-Glu<sub>15</sub>, as shown in Fig. 5(B) at the reaction coordinate of 24 Å, which is corresponding to the first peak in Fig. 4. The hydrogen bond Gly<sub>158</sub>-O··HN-Arg<sub>17</sub> is broken

(Fig. 5(C)) when the force reaches the second peak in Fig. 3. When the reaction coordinate reaches 41 Å, Aggreca<sub>n</sub>\_IGD formed a new hydrogen bond with MMP8 (Gly<sub>158</sub>-NH $\cdots$ O-Ala<sub>16</sub>) (Fig. 5(D)). At the reaction coordinate of 44 Å, the newly formed hydrogen bond is broken (Fig. 5(E)). Then the hydrogen bond (Glu<sub>180</sub>-O $\cdots$ HN-Arg<sub>17</sub>) breaks right after the maximum force. Finally, the last relatively weaker hydrogen bond (occupancy less than 50%) is immediately broken (Tyr<sub>219</sub>-O $\cdots$ HN-Ile<sub>21</sub>) (Fig. 5(F)). These results reveal a three-step unbinding pathway for the MMP8-Aggreca<sub>n</sub>\_IGD complex.

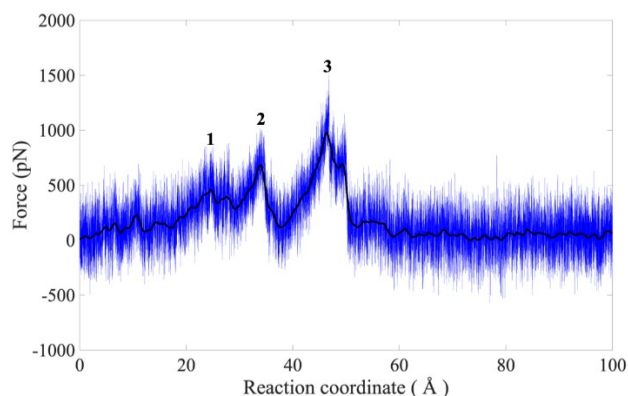
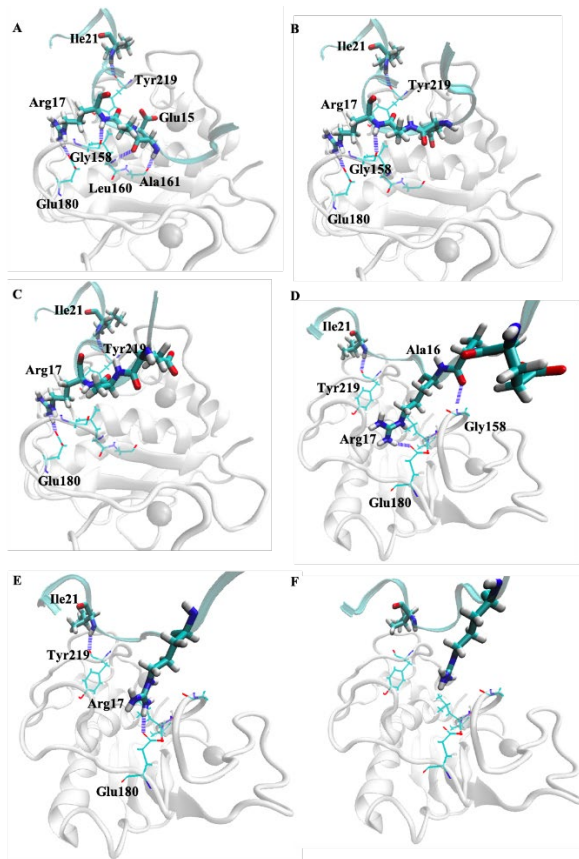


**Figure 4:** Force-reaction coordinate curve during the SMD simulations at a pulling velocity of 0.01 Å/ps

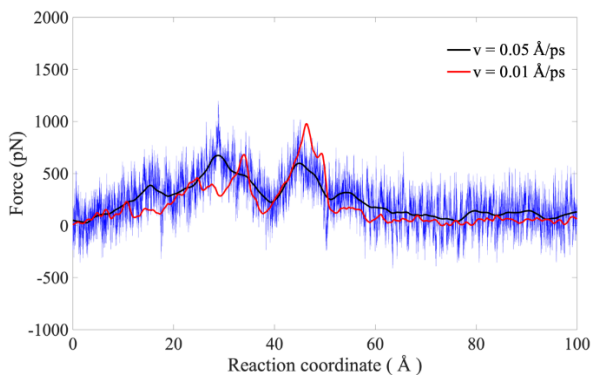
The force-reaction coordinate curve of the MMP8-Aggreca<sub>n</sub>\_IGD complex at a pulling velocity of 0.05 Å/ps is shown in Fig. 6. There are totally two peak forces during the SMD simulation. The first peak, which is also the maximum peak occurs at a reaction coordinate of 30 Å. The second peak appears at a reaction coordinate of 46 Å. At about 55 Å, the pulling force goes to zero.

Fig. 7 reports the unbinding pathway of the MMP8-Aggreca<sub>n</sub>\_IGD complex at the pulling velocity of 0.05 Å/ps. The initial structure of MMP8-Aggreca<sub>n</sub>\_IGD complex is showing in Fig. 7(A). Aggreca<sub>n</sub>\_IGD loses two hydrogen bonds (Ala<sub>161</sub>-O $\cdots$ HN-Glu<sub>15</sub> and Leu<sub>160</sub>-NH $\cdots$ O-Glu<sub>15</sub>) (seen Fig. 7(B)) at the reaction coordinate of 30 Å where the maximum force appears. When the reaction coordinate reaches 46 Å, the other two hydrogen bonds (Glu<sub>180</sub>-O $\cdots$ HN-Arg<sub>17</sub> and Gly<sub>158</sub>-O $\cdots$ HN-Arg<sub>17</sub>) are broke (Fig. 7(C)) corresponding to the second peak in Fig. 6. The last hydrogen bond is also broken immediately (Fig. 7(D)). These results reveal a two-step unbinding pathway for the MMP8-Aggreca<sub>n</sub>\_IGD complex at a higher pulling velocity.

In summary, the unbinding pathway of the MMP8-Aggreca<sub>n</sub>\_IGD complex is altered by the deformation rate. When the pulling velocity is lower, the mechanical force required to unbind the Aggreca<sub>n</sub>\_IGD from MMP8 is higher, and a three-step unbinding pathway is observed. On the other hand, when the pulling velocity is higher, the mechanical force required to unbind the Aggreca<sub>n</sub>\_IGD from MMP8 is lower, and a two-step unbinding pathway is observed. The specific transition state (Fig. 5(D)) in the unbinding pathway is observed at a lower pulling velocity.



**Figure 5:** Unbinding pathway of the MMP8-Aggregan\_IGD complex at the pulling velocity of  $0.01 \text{ \AA/ps}$ . MMP8 is rendered in white NewCartoon, and Aggregan\_IGD is rendered in licorice. Dashed lines mean the hydrogen bonds between MMP8 and Aggregan\_IGD [Humphrey, Dalke and Schulten (1996)]



**Figure 6:** Force-reaction coordinate curve during the SMD simulations at the pulling velocity of  $0.05 \text{ \AA/ps}$ . The smoothed force-reaction coordinate curve at the pulling velocity of  $0.01 \text{ \AA/ps}$  is represented in red color

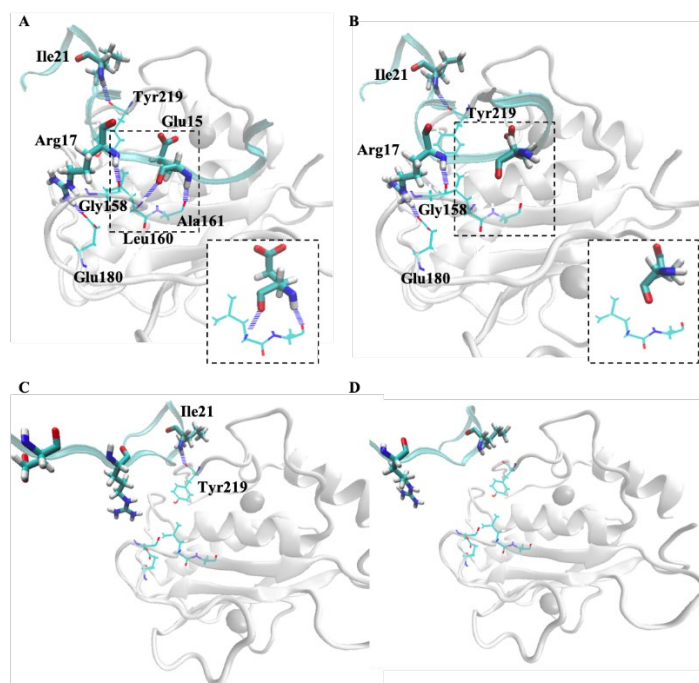


**Figure 7:** Unbinding pathway of MMP8-Aggregan\_IGD complex at the pulling velocity of 0.05 Å/ps. MMP8 is rendered in white NewCartoon, and Aggregan\_IGD is rendered in licorice. Dashed lines mean hydrogen bonds between MMP8 and Aggregan\_IGD [Humphrey, Dalke and Schulten (1996)]

### 3.3 Effects of different force constant on the potential of mean force (PMF)

As the discussion above, the unbinding pathway of MMP8-Aggregan\_IGD complex is controlled by the deformation rate. The transition state (Fig. 5(D)) is only observed at lower pulling velocity. To further study the influence of the force constants as Aggregan\_IGD unbinding MMP8 at lower pulling velocity (0.01 Å/ps), PMF is calculated to estimate the free energy during the unbinding pathway with different force constants ( $K=0.597$  kcal/mol/Å<sup>2</sup>,  $K=7$  kcal/mol/Å<sup>2</sup>). The PMF in Fig. 8 shows the energy change along the unbinding pathway of the MMP8-Aggregan\_IGD complex. When  $K=0.597$  kcal/mol/Å<sup>2</sup>, PMF increases slightly at the beginning mainly due to the hydrogen bonds of Ala<sub>161</sub>-O···HN-Glu<sub>15</sub> and Leu<sub>160</sub>-NH···O-Glu<sub>15</sub> until 35 Å. Then the PMF increases sharply until 55 Å due to the hydrogen bonds of Glu<sub>180</sub>-O···HN-Arg<sub>17</sub> and Gly<sub>158</sub>-O···HN-Arg<sub>17</sub>. Finally, the PMF is converged after 95 Å displacement. As for  $K=7$  kcal/mol/Å<sup>2</sup>, PMF increases slightly at the beginning also because of the hydrogen bonds of Ala<sub>161</sub>-O···HN-Glu<sub>15</sub> and Leu<sub>160</sub>-NH···O-Glu<sub>15</sub> until 31 Å displacement. Then the PMF increased sharply until 48 Å displacement also due to the hydrogen bonds of Glu<sub>180</sub>-O···HN-Arg<sub>17</sub> and Gly<sub>158</sub>-O···HN-Arg<sub>17</sub>. Finally, the PMF is converged after 96 Å displacement. Both PMF profiles have similar free energy change during the unbinding pathway of the MMP8-Aggregan\_IGD complex, suggesting that force constants do not affect the PMF significantly at a relatively lower pulling velocity.

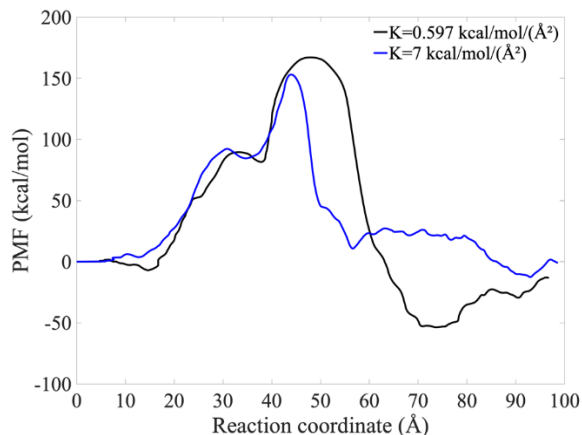


**Figure 8:** Potential of Mean Force of the SMD simulations at different force constant

#### 4 Conclusion

By using the full atomistic simulation approach, we investigate the effects of mechanical force on the unbinding pathway of the MMP8-Aggreca\_n\_IGD complex from the atomistic scale. We find that the pulling velocity alters the unbinding pathway of MMP8-Aggreca\_n\_IGD complex. When the pulling velocity is slow, the mechanical force required to unbind the Aggreca\_n\_IGD from MMP8 is higher, and a three-step unbinding pathway is observed. On the other hand, when the pulling velocity is fast, the mechanical force required to unbind the Aggreca\_n\_IGD from MMP8 is lower, and a two-step unbinding pathway is observed. An additional transition state with a new hydrogen bond forming between the MMP8 and the Aggreca\_n\_IGD along the unbinding pathway is observed only at the lower pulling velocity. We also investigate the effects of the force constant on the PMF estimation along the unbinding pathway. We found that the PMF profiles obtained with a different force constant have similar free energy change along the unbinding pathway of MMP8-Aggreca\_n\_IGD complex. This indicates that force constant has a relatively low influence for the PMF calculation. This study helps us to understand how the pulling velocity and force constant of SMD affects the unbinding pathway of the MMP8-Aggreca\_n\_IGD complex at the molecular level.

**Acknowledgments:** The authors appreciate the financial support from the Ministry of Science and Technology (107-2218-E-002-064 and 108-2636-E-002-016), Taiwan (R.O.C). We are grateful to the National Center for High-performance Computing for computer time and facilities.

#### References

Aprodu, I.; Redaelli, A.; Soncini, M. (2008): Actomyosin interaction: mechanical and energetic properties in different nucleotide binding states. *International Journal of Molecular Sciences*, vol. 9, no. 10, pp. 1927-1943.

- Bassey, E. J.; Rothwell, M. C.; Littlewood, J. J.; Pye, D. W.** (1998): Pre- and postmenopausal women have different bone mineral density responses to the same high-impact exercise. *Journal of Bone and Mineral Research*, vol. 13, no. 12, pp. 1805-1813.
- Bertini, I.; Calderone, V.; Fragai, M.; Luchinat, C.; Maletta, M. et al.** (2006): Snapshots of the reaction mechanism of matrix metalloproteinases. *Angewandte Chemie-International Edition*, vol. 45, no. 47, pp. 7952-7955.
- Borrelli, J.; Torzilli, P. A.; Grigiene, R.; Helfet, D. L.** (1997): Effect of impact load on articular cartilage: development of an intra-articular fracture model. *Journal of Orthopaedic Trauma*, vol. 11, no. 5, pp. 319-326.
- Buckwalter, J. A.** (2012): The role of mechanical forces in the initiation and progression of osteoarthritis. *HSS Journal*, vol. 8, no. 1, pp. 37-38.
- Capelli, A. M.; Costantino, G.** (2014): Unbinding pathways of VEGFR2 inhibitors revealed by steered molecular dynamics. *Journal of Chemical Information and Modeling*, vol. 54, no. 11, pp. 3124.
- Colizzi, F.; Perozzo, R.; Scapozza, L.; Recanatini, M.; Cavalli, A.** (2010): Single-molecule pulling simulations can discern active from inactive enzyme inhibitors. *Journal of the American Chemical Society*, vol. 132, no. 21, pp. 7361.
- Crooks, G. E.** (2000): Path-ensemble averages in systems driven far from equilibrium. *Physical Review E*, vol. 61, no. 3, pp. 2361-2366.
- Dellago, C.; Hummer, G.** (2013): Computing equilibrium free energies using non-equilibrium molecular dynamics. *Entropy*, vol. 16, no. 1, pp. 41-61.
- Durigova, M.; Nagase, H.; Mort, J. S.; Roughley, P. J.** (2011): MMPs are less efficient than ADAMTS5 in cleaving aggrecan core protein. *Matrix Biology*, vol. 30, no. 2, pp. 145-153.
- Ewers, B. J.; Dvoracek-Driksna, D.; Orth, M. W.; Haut, R. C.** (2001): The extent of matrix damage and chondrocyte death in mechanically traumatized articular cartilage explants depends on rate of loading. *Journal of Orthopaedic Research*, vol. 19, no. 5, pp. 779-784.
- Ewers, B. J.; Jayaraman, V. M.; Banglmaier, R. F.; Haut, R. C.** (2003): Rate of blunt impact loading affects changes in retropatellar cartilage and underlying bone in the rabbit patella (vol. 35, pp. 747, 2002). *Journal of Biomechanics*, vol. 36, no. 1, pp. 151-152.
- Felson, D. T.** (2013): Osteoarthritis as a disease of mechanics. *Osteoarthritis Cartilage*, vol. 21, no. 1, pp. 10-15.
- Ferreira, M. F. J.; Franca, E. F.; Leite, F. L.** (2017): Unbinding pathway energy of glyphosate from the EPSPs enzyme binding site characterized by Steered Molecular Dynamics and Potential of Mean Force. *Journal of Molecular Graphics and Modelling*, vol. 72, pp. 43-49.
- Fiser, A.; Sali, A.** (2003): MODELLER: generation and refinement of homology-based protein structure models. *Macromolecular Crystallography Pt D*, vol. 374, pp. 461-491.
- Fosang, A. J.; Rogerson, F. M.; East, C. J.; Stanton, H.** (2008): ADAMTS-5: the story so far. *European Cells & Materials*, vol. 15, pp. 11-26.

- Grodzinsky, A. J.; Levenston, M. E.; Jin, M.; Frank, E. H.** (2000): Cartilage tissue remodeling in response to mechanical forces. *Annual Review of Biomedical Engineering*, vol. 2, pp. 691-713.
- Hu, G.; Xu, S.; Wang, J.** (2015): Characterizing the free-energy landscape of MDM2 protein-ligand interactions by steered molecular dynamics simulations. *Chemical Biology & Drug Design*, vol. 86, no. 6, pp. 1351-1359.
- Huang, K.; Wu, L. D.** (2008): Aggrecanase and aggrecan degradation in osteoarthritis: a review. *Journal of International Medical Research*, vol. 36, no. 6, pp. 1149-1160.
- Humphrey, W.; Dalke, A.; Schulten, K.** (1996): VMD: Visual molecular dynamics. *Journal of Molecular Graphics & Modelling*, vol. 14, no. 1, pp. 33-38.
- Jarzynski, C.** (1997): Equilibrium free-energy differences from nonequilibrium measurements: a master-equation approach. *Physical Review E*, vol. 56, no. 5, pp. 5018-5035.
- Jo, S.; Cheng, X.; Islam, S. M.; Huang, L.; Rui, H. et al.** (2014): CHARMM-GUI PDB manipulator for advanced modeling and simulations of proteins containing nonstandard residues. *Advances in Protein Chemistry and Structural Biology*, vol. 96, pp. 235-265.
- Julkunen, P.; Harjula, T.; Iivarinen, J.; Marjanen, J.; Seppanen, K. et al.** (2009): Biomechanical, biochemical and structural correlations in immature and mature rabbit articular cartilage. *Osteoarthritis Cartilage*, vol. 17, no. 12, pp. 1628-1638.
- Kalva, S.; Azhagiya Singam, E. R.; Rajapandian, V.; Saleena, L. M.; Subramanian, V.** (2014): Discovery of potent inhibitor for matrix metalloproteinase-9 by pharmacophore based modeling and dynamics simulation studies. *Journal of Molecular Graphics and Modelling*, vol. 49, pp. 25-37.
- MacKerell, A. D.; Bashford, D.; Bellott, M.; Dunbrack, R. L.; Evanseck, J. D. et al.** (1998): All-atom empirical potential for molecular modeling and dynamics studies of proteins. *Journal of Physical Chemistry B*, vol. 102, no. 18, pp. 3586-3616.
- Malemud, C. J.** (2017): Matrix metalloproteinases and synovial joint pathology. *Progress in Molecular Biology and Translational Science*, vol. 148, pp. 305-325.
- Muller, G. M.; Seddon, H. J.** (1953): Late results of treatment of congenital dislocation of the hip. *Journal of Bone and Joint Surgery-British Volume*, vol. 35, no. 3, pp. 342-362.
- Niu, Y.; Li, S.; Pan, D.; Liu, H.; Yao, X.** (2016): Computational study on the unbinding pathways of B-RAF inhibitors and its implication for the difference of residence time: insight from random acceleration and steered molecular dynamics simulations. *Physical Chemistry Chemical Physics*, vol. 18, no. 7, pp. 5622-5629.
- O'Kane, J. W.; Hutchinson, E.; Atley, L. M.; Eyre, D. R.** (2006): Sport-related differences in biomarkers of bone resorption and cartilage degradation in endurance athletes. *Osteoarthritis Cartilage*, vol. 14, no. 1, pp. 71-76.
- Patel, J. S.; Berteotti, A.; Ronsisvalle, S.; Rocchia, W.; Cavalli, A.** (2014): Steered molecular dynamics simulations for studying protein-ligand interaction in cyclin-dependent kinase 5. *Journal of Chemical Information and Modeling*, vol. 54, no. 2, pp. 470-480.
- Phillips, J. C.; Braun, R.; Wang, W.; Gumbart, J.; Tajkhorshid, E. et al.** (2005): Scalable molecular dynamics with NAMD. *Journal of Computational Chemistry*, vol. 26, no. 16, pp. 1781-1802.

**Pratta, M. A.; Yao, W.; Decicco, C.; Tortorella, M. D.; Liu, R. Q. et al.** (2003): Aggrecan protects cartilage collagen from proteolytic cleavage. *Journal of Biological Chemistry*, vol. 278, no. 46, pp. 45539-45545.

**Pufe, T.; Lemke, A.; Kurz, B.; Petersen, W.; Tillmann, B. et al.** (2004): Mechanical overload induces VEGF in cartilage Discs via Hypoxia-Inducible factor. *American Journal of Pathology*, vol. 164, no. 1, pp. 185-192.

**Renaux, A.; Consortium, U.** (2018): UniProt: the universal protein knowledgebase. *Nucleic Acids Research*, vol. 46, no. 5, pp. 2699.

**Sanner, M. F.; Olson, A. J.; Spohner, J. C.** (1996): Reduced surface: An efficient way to compute molecular surfaces. *Biopolymers*, vol. 38, no. 3, pp. 305-320.

**Shen, J.; Li, W. H.; Liu, G. X.; Tang, Y.; Jiang, H. L.** (2009): Computational insights into the mechanism of ligand unbinding and selectivity of estrogen receptors. *Journal of Physical Chemistry B*, vol. 113, no. 30, pp. 10436-10444.

**Shen, M.; Guan, J.; Xu, L.; Yu, Y.; He, J. et al.** (2012): Steered molecular dynamics simulations on the binding of the appendant structure and helix-beta2 in domain-swapped human cystatin C dimer. *Journal of Biomolecular Structure and Dynamics*, vol. 30, no. 6, pp. 652-661.

**Shen, Z.; Cheng, F.; Xu, Y.; Fu, J.; Xiao, W. et al.** (2012): Investigation of indazole unbinding pathways in CYP2E1 by molecular dynamics simulations. *PLoS One*, vol. 7, no. 3, e33500.

**Tekpinar, M.** (2018): Steered molecular dynamics simulations of coumarin2 5Z/5E pulling reveal different interaction profiles for four human cytosolic carbonic anhydrases. *Süleyman Demirel Üniversitesi Fen Bilimleri Enstitüsü Dergisi*, vol. 22, no. 2.

**Truong, D. T.; Li, M. S.** (2018): Probing the binding affinity by Jarzynski's nonequilibrium binding free energy and rupture time. *Journal of Physical Chemistry B*, vol. 122, no. 17, pp. 4693-4699.

**Vashisth, H.; Abrams, C. F.** (2008): Ligand escape pathways and (un)binding free energy calculations for the hexameric insulin-phenol complex. *Biophysical Journal*, vol. 95, no. 9, pp. 4193-4204.

**Venn, M.; Maroudas, A.** (1977): Chemical composition and swelling of normal and osteoarthrotic femoral head cartilage. I. Chemical composition. *Annals of the Rheumatic Diseases*, vol. 36, no. 2, pp. 121-129.

**West, D. K.; Olmsted, P. D.; Paci, E.** (2006): Free energy for protein folding from nonequilibrium simulations using the Jarzynski equality. *Journal of Chemical Physics*, vol. 125, no. 20, 204910.

**Xu, L.; Hasin, N.; Shen, M.; He, J.; Xue, Y. et al.** (2013): Using steered molecular dynamics to predict and assess Hsp70 substrate-binding domain mutants that alter prion propagation. *PLoS Computational Biology*, vol. 9, no. 1, e1002896.

**Xue, Y. L.; Zhou, L.; Sun, Y.; Li, H.; Jones, G. W. et al.** (2017): Steered molecular dynamics simulation of the binding of the bovine auxilin J domain to the Hsc70 nucleotide-binding domain. *Journal of Molecular Modeling*, vol. 23, no. 11, pp. 320.

**Zhang, J.; Zheng, Q.; Zhang, H.** (2010): Unbinding of glucose from human pulmonary surfactant protein D studied by steered molecular dynamics simulations. *Chemical Physics Letters*, vol. 484, no. 4-6, pp. 338-343.

**Zhang, W.; Wang, M. L.; Cranford, S. W.** (2016): Ranking of molecular biomarker interaction with targeted DNA nucleobases via full atomistic molecular dynamics, *Scientific Reports*, vol. 6, pp. 18659.

**Zhang, Z.; Santos, A. P.; Zhou, Q.; Liang, L.; Wang, Q. et al.** (2016): Steered molecular dynamics study of inhibitor binding in the internal binding site in dehaloperoxidase-hemoglobin. *Biophysical Chemistry*, vol. 211, pp. 28-38.